https://doi.org/10.5194/egusphere-2025-5369
Preprint. Discussion started: 21 January 2026

Distinct atmospheric drivers of Ross Sea coastal polynya variability during winter

Girija Kalyani Burada[1,2], James Renwick[1], and Adrian McDonald[3]

[1] School of Geography Environment and Earth Sciences, Victoria University of Wellington, Wellington 6012, New Zealand.
[2] *Current affiliation*: Department of Earth and Planetary Sciences, Weizmann Institute of Science, Rehovot, 7610001 Israel
[3] School of Physical and Chemical Sciences, University of Canterbury, Christchurch 8041, New Zealand

Correspondence to: Girija Kalyani Burada (girija.kalyani18@gmail.com)

Abstract: Coastal polynyas in the Ross Sea have well-documented links to atmospheric circulation, but the role of specific circulation patterns in driving extreme wind events and their differential impact on individual polynyas remains poorly explored. This study examines peak-winter (Aug-Oct) variability in the Ross Sea, Terra Nova Bay, and McMurdo Sound polynyas using EOF analysis of high-resolution passive microwave sea-ice concentration data. Patterns of variability are related to surface extreme winds and 500 hPa geopotential height anomalies from ERA5, allowing concurrent assessment of local forcing and hemispheric-scale circulation connections.

Results reveal that each polynya responds differently to shifts in large-scale atmospheric features. Variations in the position and intensity of the Amundsen Sea Low, and its influence on Ross Ice Shelf Air Stream winds, are associated with marked changes in polynya area. By combining high-resolution sea ice concentration records with targeted extreme-wind analysis, this work identifies previously unresolved, location-specific atmospheric controls on Ross Sea polynya variability.

1. Introduction

Antarctic sea-ice exerts outsized influence on Southern Hemisphere and global climate through air–sea heat exchange and shelf water formation; understanding the drivers of its regional variability is therefore fundamental to projecting polar and global climate change. The Ross Sea (RS) sector is central to this issue: it exhibits one of the largest and most variable contributions to Antarctic sea-ice trends (*Yuan et al., 2017*), its polynya contribute significantly to deep-water formation and local energy budgets, and is strongly modulated by remote and regional circulation modes such as El Niño Southern Oscillation (ENSO, *Cohen et al., 2013*),, the Southern Annular Mode (SAM, *Park et al., 2018*), Zonal Wave3 (ZW3, *Goyal et al., 2021)* patterns and, crucially, shifts in the Amundsen Sea Low (ASL, *Raphael et al., 2019*).

Coastal polynyas — persistent zones of thin ice or open water adjacent to the coastline — are the proximate loci of much of the Ross Sea's variability and ice production (Mezgec et al., 2017; Tamura et al., 2008). While easy to describe in broad terms, they are complex features of the sea-ice field, and their behaviour can be difficult to interpret from satellite soundings. Field campaigns and process studies (e.g., *Ackley et al., 2020; Guest, 2021; Thompson et al., 2020*) emphasise that polynyas are internally structured: an open-water/frazil-ice production zone, an accumulation/rafted-pancake zone, and a young-floe zone, and that most of the new ice formation and heat fluxes are confined to the active frazil/open-water zones. This physical zoning explains why coarse or poorly validated satellite retrievals can misrepresent the processes that make polynyas "ice-production factories" (*Martin et al., 2004; Bradtke & Herman, 2023*). At the same time, studies focusing on frazil and active ice production (*Tamura et al., 2008; Nakata et al., 2021*) highlight that estimates of polynya characteristics are highly sensitive to the spatial resolution and retrieval approach used. Higher-resolution datasets and algorithms tuned to detect thin or newly forming ice can capture the fine-scale variability within the polynya, whereas coarse or generalized methods often underestimate its true area and ice production rate.

A large body of work links near-surface winds and synoptic circulation to polynya behaviour in the RS. Strong offshore katabatic and synoptic winds drive dynamic ice export and sustain the Ross Ice Shelf Air Stream (RAS), producing characteristic episodes of ice advection and polynya opening (*Dale et al., 2017; Coggins & McDonald, 2015; Seefeldt et al., 2007*). Other studies document extreme, event-scale responses — for example, the dramatic expansion of the Terra Nova Bay polynya during cyclone-driven wind events (*Wenta & Cassano, 2020*) — and show how large-scale modes such as a displaced ASL modulate the frequency and intensity of these wind regimes (*Raphael et al., 2016;*). Yet despite these advances, two important limitations remain in the literature.

First, most process-level studies that validate the physics of frazil formation and air–sea fluxes (e.g., *Ackley et al., 2020; Guest, 2021; Thompson et al., 2020)* are necessarily limited in time and spatial coverage — they provide excellent snapshots but cannot by themselves characterise interannual to decadal variability. Second, longer-term statistical and remote sensing studies have typically sacrificed spatial resolution for record length: coarser (≈25 km) passive microwave products and large-scale indices are useful for trends but do not reliably resolve the narrow frazil or young-floe bands that control production and the detailed footprint of katabatic and barrier winds (*Burada et al., 2023,* also refer Figure S1). Conversely, newer high-resolution approaches that can resolve frazil signatures or use active sensors (e.g., Sentinel-1 SAR, *Nakata et al., 2021; Tamura et al., 2008*) either cover shorter time windows or are spatially fragmented, complicating assessments of long-term and large-scale change.

There are three clear gaps to address: (i) We lack a long-term, high-spatial-resolution view of how the same local polynyas; Ross Sea Polynya (RSP), Terra Nova Bay Polynya (TNBP), McMurdo Sound Polynya (MCMP) respond across years to systematic shifts in large-scale circulation. (ii) There is limited synthesis that links field-observed process zones (frazil/accumulation/young floe) to satellite-derived sea ice concentration (SIC) patterns and to the synoptic and upper-level flow that modulates extreme winds. (iii) many statistical studies quantify correlations between circulation indices and polynya area but stop short of resolving the multi-scale pathway (Large-scale circulation → Extreme surface winds → local sea-ice advection), and they often over-interpret observational data (melting vs. inhibited freeze-up) without reconciling process measurements.

This study directly targets those gaps. Using a 20-year SIC record at ~6.25 km resolution — combined with an extreme-wind metric and 500-hPa geopotential fields from ERA5 — we provide the first comprehensive multi-decadal, high-resolution analysis that: (a) examines all three major Ross Sea coastal polynyas together, (b) explicitly links upper-level circulation anomalies to event-scale extreme winds and to the spatial fingerprint of thin-ice/open-water bands. Using combined statistical techniques to quantify co-variability across scales, and by treating SIC anomalies as proxies for thin-ice/open-water bands (with careful discussion of existing passive microwave dataset limitations), we bridge the timescale/resolution divide and provide mechanistic — not merely correlative — evidence that large-scale circulation shifts modulate polynya behaviour via their control of extreme coastal winds.

In short; previous work has either resolved processes at high fidelity over short periods or produced long records at coarse resolution; our contribution is to join these strengths — multi-decadal perspective, process-aware interpretation, and sufficient spatial resolution to resolve the active frazil/young-floe bands — thereby enabling robust attribution of polynya variability to atmospheric regimes relevant for predictability and for evaluating coupled model behaviour.

2. Data and Methods

2.1. Data

Coastal polynyas in the Ross Sea operate across the late-autumn through early-spring period, but their physical character and dominant forcing mechanisms shift seasonally. The August-September-October (ASO) window (late austral winter → early spring) has three features that make it a robust target for a focused statistical study: (i) sea-ice extent is near its annual maximum so polynyas appear as persistent, coastal thin-ice/open-water bands embedded in a largely contiguous pack — this favours consistent detection in passive-microwave (PMW) time series; (ii) wind-driven dynamical processes (katabatic and synoptic offshore winds, barrier jets) are most active and repeatedly modulate ice advection and frazil-ice formation during ASO, so the atmospheric imprint is strong and interpretable; (iii) before strong surface solar forcing and the onset of intense ocean–mixed-layer warming (which grow after October), ASO minimizes competing oceanic thermodynamic influences (e.g., shelf upwelling, summer melt) that complicate attribution of polynya variability to the atmosphere. For these reasons ASO provides an optimal balance between (a) a clear atmospheric control signal, (b) reliable passive-microwave detection of thin-ice bands, and (c) reduced confounding by oceanic heat-driven processes — all of which are essential for statistical attribution of multi-scale linkages.

Daily SIC fields come from the University of Bremen ASI retrieval applied to AMSR-E (2002–2011) and AMSR-2 (2012–2022) at nominal 6.25 km grid spacing. The AMSR-E → AMSR-2 transition window (Oct 2011–Jul 2012) is excluded from analyses to avoid known calibration discontinuities. SIC fields were masked over grounded and floating ice shelves using the Antarctic Digital Database coastline (Gerrish et al., 2023) to avoid contamination from shelf ice. Hourly 10-m wind fields and 500 hPa geopotential height (H500) were obtained from ERA5 (0.25°). We derive the ExWinds metric as described below. All reanalysis fields were regridded to the SIC grid for coupled analyses (bilinear for H500 and wind components). The spatial domain for coupled analysis is 162°E–160°W, 80°S–73°S (RS sector, refer Figure 1). Analyses use ASO (August–October) daily data for 2002–2022 (excluding Oct 2011–Jul 2012), providing 19 discrete annual ASO blocks for statistical analysis.

2.2. Methods

Prior to analysis, the SIC fields were pre-processed to produce standardized anomaly time series. First, grid cells over ice shelves were masked and excluded from the dataset. Next, each retained grid-cell time series was area-weighted by the square root of its latitude, as a proxy for area ($\propto \sqrt{\cos \varphi}$) to remove latitudinal sampling bias. A daily climatology for ASO (2002–2022) was then computed by averaging data for each calendar day over a chosen reference period. A linear trend was removed from each grid point (least-squares fit) to minimize long-term bias and focus on interannual variability. The resulting detrended anomalies were divided by their temporal standard deviation (SD), calculated independently for each grid point. No additional averaging or smoothing was applied so that the data retain the short-term and regional variability important for capturing polynya-scale changes. This per-grid-point approach standardizes variability without mixing spatial and temporal variance, ensuring that all locations contribute comparably to the subsequent analysis. Finally, the daily ASO standardized anomalies from all years were concatenated in time to form the analysis matrix **S** ($N_t \times N_s$), where N_t is the total number of ASO days and N_s is the number of spatial grid points.

To capture event-scale impacts of winds (the processes most relevant to polynya opening), we compute at each ERA5 grid cell; the hourly 10 m wind speed magnitude from ERA5; the daily maximum of the hourly wind speed (i.e., the maximum 10-m wind observed during a given UTC day) — this is our ExWinds daily field; regrid ExWinds to the SIC grid and apply the same ASO climatology removal, detrending and standardization procedure as for SIC. The rationale for using daily maxima is that they better capture intense, short-lived wind events than daily means and therefore produce stronger dynamic signals in coupled analysis.

Two standard multi-variate methods are used to analyse spatial structure and coupling strength between fields:

Empirical Orthogonal Functions (EOF): Let **S** be the standardized SIC anomaly matrix ($N_t \times N_s$). We compute the spatial covariance matrix $\mathbf{C} = \mathbf{S}^T \mathbf{S}$ (N_s × N_s) and perform eigen-decomposition of

$$\mathbf{C}\, \boldsymbol{\varphi}\_k = \lambda\_k\, \boldsymbol{\varphi}\_k \qquad [1]$$

where $\boldsymbol{\varphi}$_k are spatial EOF patterns (orthonormal after area weighting) and λ_k are eigenvalues representing the variance associated with each EOF (Wilks 2011). The principal component (PC) time series for mode k is the projection $\mathbf{PC}\_k(t) = \mathbf{S}(t,:) \cdot \boldsymbol{\varphi}\_k$. The variance explained by mode k is λ_k / Σ_j λ_j. We test eigenvalue separation using North's rule of thumb (North et al., 1982) and report modes that are distinct beyond estimated sampling uncertainty.

Maximum covariance analysis (MCA): For coupled MCA (Bretherton et al 1992; Mo 2003) between SIC (**S**, N_t × N_s) and another field (**P**, N_t × N_p; e.g., ExWinds or H500), we compute

Cross-covariance matrix: $\mathbf{Cov} = \mathbf{S}^T \mathbf{P}$ (N_s × N_p) [2]

Singular value decomposition yields: $\mathbf{Cov} = \mathbf{U}\, \mathbf{L}\, \mathbf{V}^T$, [3]

where columns of **U** are the left singular vectors (spatial pattern in SIC), columns of **V** are the right singular vectors (spatial pattern in the other field), and diagonal entries l_k of **L** are singular values. The associated amplitude time series are

$$\mathbf{PC}\_{S,k}(t) = \mathbf{S}(t,:)\cdot \mathbf{U}\_k \text{ and } \mathbf{PC}\_{P,k}(t) = \mathbf{P}(t,:)\cdot \mathbf{V}\_k. \qquad [4]$$

The squared covariance fraction (SCF) for mode k is

https://doi.org/10.5194/egusphere-2025-5369
Preprint. Discussion started: 21 January 2026

$$SCF_k = \frac{l_k^2}{\Sigma\ _j l_j^2} \qquad [5]$$

and measures the fraction of total squared covariance explained by mode k.

Spatial maps shown in the paper are derived by regressing the standardized field (SIC, ExWinds, or H500) onto the normalized PC time series for each mode; this produces maps in standardized units (SD of the field) that are straightforward to compare across variables.

To verify that AMSR 6.25 km captures the same timing and broad spatial extent of polynya openings as higher-resolution sensors we performed targeted validations against Sentinel-1 SAR scenes and ARTIST-derived maps for a set of representative events (not shown). These comparisons show that 6.25 km AMSR reliably reproduces the timing and large-scale footprint of polynyas, although SAR reveals finer frazil/pancake structure within the active production band that passive-microwave retrievals show as smooth. We also performed sensitivity checks with alternative spatial weighting (no area weighting, area weighting) and with/without linear detrending; the principal modes, their interpretation, and MCA couplings are qualitatively robust across these choices. Finally, because 3.125 km-scale frazil-mapping products exist, we advise their use for event/process case studies rather than as the backbone for multi-decadal EOF/MCA, because of data set length, and we use them here only for validation and for illustrating process detail.

3. Results

3.1. Winter Sea-ice concentration (SIC) and EOFs

The average winter SIC (Figure 1a) is broadly uniform across the RS except in the three coastal polynya regions, which exhibit markedly lower mean SIC (~50%, green shading). The variability map in Figure 1b displays the aggregated ASO daily SD, defined as the standard deviation of all daily SIC anomaly values during ASO across 2002–2022 (within-season, day-to-day variability aggregated across all years;). This clearly highlights enhanced variability concentrated within the RSP, TNBP, and MCMP domains. In contrast, regions of compact, stable winter pack ice (e.g., central RS) maintain SIC persistently close to 100% during ASO, resulting in very low SD values (often <3%). These low values reflect the physical stability of the ice cover. A 12% SD threshold (black dashed line in Figure 1b) is used to delineate the spatial extent of polynya domains for subsequent analyses.

The spatial patterns of SIC variability were extracted using EOF analysis applied to the standardized ASO SIC anomaly fields. The first three EOFs (Figure 2) are statistically significant (Figure S2) by the North et al. (1982) criterion and together explain 37% of the total SIC variance within the RS coastal domain. In geophysical datasets, such explained variance is typical — the leading modes isolate the most coherent, physically interpretable large-scale patterns, whereas the remaining variance is a mix of higher-order spatial variability, localised processes, and stochastic noise (Figure S3). EOF 1 (Figure 2a) captures a coherent mode of variability encompassing all three major polynyas, with spatial anomalies closely matching the high-variability regions identified by the 12 % SD threshold in Figure 1b. Its PC time series (PC1) shows a notable increase after 2015, consistent with a recent reduction in SIC across these polynya zones. The spatial patterns two and three (Figure 2b and 2c) capture opposing behaviours in sea-ice distribution within the SD boundary of RSP, seen as north-south and east-west variances. The second pattern (Figure 2b), with 7.6% variance displays lower concentrations of sea ice over the western portion of the RSP and over the MCMP. However, opposite effects are on the eastern

https://doi.org/10.5194/egusphere-2025-5369
Preprint. Discussion started: 21 January 2026

RS and the TNBP region with higher SICs. MCMP variations dominate in this pattern. A north-south dipole centred around Ross Island within RSP (black dotted lines in Figure 1), can be seen here. Increased sea-ice in Eastern RS and TNBP regions, co-occur with decreased sea-ice in MCMP and east of Ross Island. Pattern three (Figure 2c), with 7.4% of the variance, is close to the second pattern in terms of variance accounted for. Within the SD boundary, east-west split in RS region, with a clear polynya activity in Western Ross Sea (WRS). This pattern highlights lower concentration of sea ice in the western portion of RS and opposite anomalies over eastern RS. PCs associated 3 show increases in 2015-2018 implying SIC decreases over WRS.

EOF 2 and EOF 3 have similar eigenvalues, suggesting they may represent mixed modes — i.e., different linear combinations of these patterns can capture similar variance. By focusing on EOF 1–3, we retain the dominant, spatially robust patterns most relevant to RSP variability, while acknowledging that the remaining 63 % of variance contains smaller-scale and transient processes beyond the scope of this EOF-based framework.

3.2. Circulation variability and sea-ice

3.2.1. Role of Extreme Winds in RS polynya dynamics during ASO

The relationship between ExWin and SIC is analysed using MCA. MCA Mode 1 (Figure 3A(a) and 3A(d), 73% SCF) reveals a relationship characterised by intense (seen as positive anomalies in ExWin) wind speed anomalies over the three polynyas and the RIS (dashed box in Figure 3), along with a pronounced low-level jet (the RAS) near the southern Siple Coast (Figure 3A(d)). This wind configuration presumably drives SIC reductions particularly over central RS, through enhanced ice advection. Strengthened southerly (northerly) winds exert strong offshore transport, dynamically forcing the surface ice away from the coast (towards) resulting in reduced (higher) SIC near close to the coast, in polynya zones. These southerly winds directed onto the central part of RIS are associated with the RAS pattern (Figure 3B). As MCA patterns are sign-independent, reversing the sign (or colours) would invert the interpretation without altering the underlying physical relationship. The associated PCs from ExWin are correlated with PCs of large-scale wind vectors (Figure 3B: MCA of ExWin/WinVec), by a coefficient of 0.83. Given the large SCF, this coupling clearly dominates SIC variability in the three polynya regions during winters.

Mode 2 between SIC and ExWinds (Figure 3A(b,e); 15 % SCF) is characterised by lower SICs in eastern RSP and TNBP under weak or light winds. These conditions are associated with an anticyclonic circulation that reorients the flow into a northwest–southeast pattern (Figure 3B(e)), weakening the katabatic outflows that normally sustain high ice divergence and export in these polynyas. Although weaker winds are generally associated with reduced ice divergence, in this mode the decrease in katabatic strength may coincide with a reorientation of wind flow into a northwest–southeast pattern. This shift could alter ice drift perhaps advecting ice away from certain coastal sectors even under weaker forcing (*Holland & Kwok, 2012; Dale et al., 2017*). At the same time, suppressed turbulence and surface cooling may inhibit frazil ice formation and delays freeze-up (*Ackley et al., 1990; Thompson et al., 2020*), allowing open-water or thin-ice areas to persist. Later in the ASO season, these calm conditions may also enhance shortwave absorption, further delaying refreeze (*Stammerjohn et al., 2008*). Thus, the apparent SIC reductions under weak-wind conditions presumably reflect a combination of dynamical (drift reorientation) and thermodynamic (slower ice growth) effects, consistent with the anticyclonic or weak-synoptic regime typical of the RS. The observed accumulation and higher SIC near MCMP are consistent

https://doi.org/10.5194/egusphere-2025-5369
Preprint. Discussion started: 21 January 2026

with wind-driven convergence and mechanical thickening in this sector. These patterns align with RS regime classifications (*Seefeldt et al., 2007; Coggins & McDonald, 2015*) that identify anticyclonic or weak-synoptic states as conducive to altered drift and redistribution. While MCA diagnoses statistical coupling rather than causation, the spatial and temporal consistency with known RS dynamics provides a robust physical basis for the interpretation.

Mode 3 (Figure 3c & 3f; 5 % SCF) represents a circulation regime influenced by the Barrier Wind Corner Jet (BWCJ) mechanism, where strong southerly barrier winds approaching Ross Island are deflected and accelerated as they round the Ross Island's eastern flank (*Seefeldt, 2012*). This process results from the interaction of large-scale flow with the steep topography of Ross Island, causing the wind to split into two branches — one flowing eastward along the RIS front and the other curving northward along the eastern RS. Although Mode 3's wind origin along the Siple Coast resembles Mode 1 (Figure 3d), ExWin weakens slightly before reaching Ross Island, then intensifies sharply near the island's eastern tip presumably due to BWCJ acceleration. We suggest this enhanced flow drives rapid offshore advection of sea ice east of Ross Island, lowering SIC locally and transporting ice equatorward. In the ASO season, this impact is most likely predominantly dynamical — involving increased ice divergence and redistribution — rather than thermodynamic melt, since both air and ocean temperatures over the RS continental shelf remain at or near the freezing point (*Jacobs & Giulivi, 1998; Williams et al., 2010*). While strong winds can enhance local air–sea coupling where thin ice or open water is created, the net effect during late winter is the mechanical removal and displacement of ice, occasionally followed by new-ice formation in exposed areas (*Bromwich et al., 1998; Massom et al., 1998; Parish et al., 2006; Nicolas & Bromwich, 2011).* The MCA-derived SIC pattern for Mode 3 correlates with EOF3 (r ≈ 0.69), confirming that this barrier-wind-dominated mode captures a distinct and coherent component of SIC variability in the Ross Island sector.

Altogether 93% of the squared covariance between ExWinds and associated polynya is captured in this analysis. Modes one and three suggest different regimes of ExWin that intricately modulate RAS during different period of evolution. ExWinds patterns play a very strong role in modulating the three polynya regions of the RS. The origin of extreme winds arriving at RIS are evidently influenced by atmospheric dynamics around the RS. It is also worth noting, that in our localized analysis of MCA analysis with wind vectors and ExWin (not shown), we were unable to capture the BWCJ wind regime.

3.2.2. Role of large-scale circulation in polynya dynamics in the RS

To explore the role of large-scale circulation variability on ExWinds of RS we carried out another MCA analysis between H500 and ExWinds (H500/ExWinds).

The first mode of H500-ExWinds coupling (Figure 4(a)/(d), SCF 46%) displays a significant anomaly to the northeast of the RS (Figure 4d). This pattern resembles an ASL pattern in H500 fields, with its centre shifted westward from its climatological position near ~110° W toward ~ 150^0 W over the eastern RS (*Turner et al., 2013*), and extending eastward across the Amundsen - Bellingshausen Sea. This positioning would steer surface cyclones onto the RS (*Coggins & McDonald, 2015*) and is consistent with enhanced southerly flow impinging on the central shelf region. The H500 anomaly pattern is associated with decreased SIC (Figure 4g), presumably through the modulation of local winds that favour northward advection of ice. The polarity of this relationship is sign-independent though and could equally be interpreted as a northerly flow associated with higher SIC. This circulation pattern may correspond to the RAS pattern identified in Figure 3(d) with the low H500 centre likely inducing a south-to-southeasterly flow over the central RS and weaker activity in the western sector, leading to a dominant RSP. Figure 4(g) is derived from regressing the PCs of ExWin pattern (Figure 4a) onto the SIC field, which mirrors the spatial pattern of EOF1 reinforcing the coherent coupling between large-scale circulation, surface winds, and sea-ice variability.

Mode two (Figure 4(b) and 4(e): SCF 21%) is characterised by a deep low (negative H500 anomaly) near the Antarctic Peninsula (AP) with a positive H500 anomaly over the WRS, a dipole pattern over West Antarctica. The positive H500 anomaly (high-pressure system) is usually associated with calm and stable environments, bringing anticyclonic winds over the RS. The anticyclonic winds, traveling from west to east across the northern RS, appears subdued in speed, as indicated by weak ExWin anomalies, consistent with the reduced pressure gradients characteristic of high-pressure systems. These weaker winds may contribute to reduced wind-driven ice export and likely influence sea-ice redistribution, perhaps removing ice from the TNBP and eastern RS sectors (Figure 4h) and enhancing ice divergence that lowers SIC. In this redistribution, ice is piled up near MCMP, hence positive SIC anomalies. Under such calm, high-pressure regimes, the absence of strong wind forcing probably slows the formation of new ice in recently opened water by reducing turbulent heat loss and frazil ice production, allowing thin ice or open-water areas to persist for longer (*Drucker et al., 2003; Morales Maqueda et al., 2004; Fusco et al., 2009*). This process, combined with altered advection, may explain the observed lower SIC in TNBP and eastern RS and the higher SIC in MCMP. Thus, Mode 2 reflects a coupled dynamic–thermodynamic response in which anticyclonic, weak-wind conditions drive redistribution of sea ice and modify freeze-up rates, producing the spatial SIC variability observed in Figure 4(h).

Mode three (Figure 4c and 4f: SCF ~11%) displays a positive H500 anomaly over the RS centred near Cape Colbeck (Figure 4f), possibly related to blocking. The upper-level ridge (positive H500) modulates the BWCJ regime. Blocking of stably stratified air by the barrier causes imbalance, the creation of a terrain-induced region of high pressure. The BWCJ forms when a stably stratified low-level airflow along the base of the Transantarctic Mountains (TAM) interacts with the topographical barrier imposed by Ross Island. The wind intensifies and flows towards the north-west. Most of the flow passes on the right side of Ross Island, whereas a minimal amount of the flow passes on the left (Figure 4f). This deflection is because of the balance between the pressure gradient force and the Coriolis force. The development of BWCJ is often associated with mesoscale cyclones (*Carrasco & Bromwich,1993*). The high-pressure H500 anomalies or the blocking patterns may relate to tropically induced Rossby wave trains resulting in strong ENSO modulation in this region (*Renwick, 2005*) but are not discussed further. Therefore, the positioning of the H500 gradients to TAM modulates different wind regimes onto RS region.

Together 78% of squared covariability between extreme winds and H500 field is captured here, emphasizing the importance of the position of larger scale H500 anomalies influencing surface winds in the RS region. We therefore demonstrate the potential for the upper-level circulation in controlling the intricate local wind regimes in RS region. These patterns of large-scale H500 anomalies and associated maximum surface winds are clearly linked to with sea-ice distributions in winter within each of the polynya regions.

4. Discussions

Our MCA/EOF results lead us to postulate that RS polynya variability during the ASO season is dominated by a small set of coupled modes in which upper-level circulation anomalies (H500) modulate local extreme winds (ExWin), and those wind regimes in turn control the spatial footprint of thin-ice/open-water bands inferred from SIC. Mode 1 is characterised by intensified katabatic/southerly RAS flows that export sea-ice northward and expand the RSP; Mode 2 corresponds to anticyclonic/weak-wind regimes that favour lateral spreading/accumulation near McMurdo and relative opening in TNBP; Mode 3 reflects BWCJ behaviour around Ross Island that drives lateral sea-ice advection eastwards. These interpretations emphasise dynamic ice export and inhibited freeze-up (i.e., delayed new-ice formation) as the proximate mechanisms for polynya area changes in ASO, consistent with targeted process observations (PIPERS, *Ackley et al., 2020*) and recent detailed katabatic jet studies (*Guest 2021; Thompson et al., 2020*).

The strong negative phase in EOF1 after 2016 coincides with the well-documented Antarctic-wide decline in winter sea ice, suggesting that the RS response forms part of this broader shift. While the immediate reduction in SIC may be linked to the enhanced wind events and associated ASL displacements. the persistence of these anomalies likely reflects coupled atmosphere–ocean processes. This is also supported by recent multi-year and decadal studies that show polynya behaviour is not only event-driven but also modulated on interannual to multi-decadal timescales by changes in atmospheric circulation and by slowly varying ocean conditions.

Two aspects from the literature are important when placing our ASO-focused results in a broader temporal context. First, the ASL exerts a first-order control on wind regimes over the RS. Longitudinal or intensity shifts in the ASL alter the frequency and orientation of katabatic and synoptic wind patterns (e.g., RAS, barrier jets), thereby modulating the occurrence and extent of polynyas (*Raphael et al., 2016; Turner et al., 2013; Park et al., 2018*). Our Mode 1/Mode 2 distinctions map directly onto ASL displacements and dipole states, suggesting that interannual changes in ASL statistics will translate into systematic changes in polynya regime frequency — a linkage our MCA quantifies at daily-to-interannual scales.

Second, while wind forcing (atmosphere-driven) governs the timing of polynya openings, subsurface ocean processes determine their persistence. Enhanced subsurface heat content and altered stratification can delay refreezing once the ice cover is disrupted (*Zhang et al., 2022*), sustaining low SIC even under neutral atmospheric conditions. This oceanic preconditioning likely contributed to the prolonged negative anomalies in EOF1 beyond 2016. Supporting this view, large-scale analyses show interdecadal variability in polynya activity arising from interactions between ASL/SAM variability and slowly evolving oceanic states (*Duffy et al., 2024*). Together, these studies emphasize a coupled atmosphere–ocean control: atmospheric variability sets the timing, while oceanic conditions regulate the duration and magnitude of anomalies.

Our analysis captures coherent interannual variability associated with ASL-driven winds, but finer-scale processes likely underpin much of this variability. As shown by Burada et al. (*2023*), transitions between “no polynya” and “clear polynya” states can occur within a few days, highlighting their highly dynamic nature. Such short-lived events are difficult to resolve with coarse-temporal satellite products, and even Sentinel-1 SAR, despite its spatial resolution, suffers from temporal gaps that can miss strong wind events and rapid transitions. Consequently, event-scale openings may be under-sampled in multi-year records, contributing to uncertainty in trend interpretation. This underscores the need for integrated observational frameworks combining high spatial and temporal resolution to better capture the mechanisms driving polynya variability, particularly during transitions between active and quiescent states.

Our ASO-focused MCA modes robustly capture some of the dominant atmospheric pathways by which large-scale circulation anomalies modulate extreme coastal winds and thereby control ice advection and delayed freezing. However, the multi-year persistence or trends in polynya area and production likely emerge from the interaction of that atmospheric forcing with evolving ocean heat content and stratification; this explains why polynya trends seen in long records (e.g., *Park et al., 2018; Duffy et al., 2024*) can sometimes amplify or dampen the direct wind forcing signal we diagnose at daily/interannual scales.

Field campaigns and frazil-mapping research (*Tamura et al., 2008; Nakata et al., 2021; Ackley et al., 2020; Guest, 2021*) show that the active frazil/open-water band — the true engine of new ice production and latent-heat flux — is narrow and often sub-pixel for coarse retrievals. Our use of 6.25 km AMSR as a long-term backbone was chosen to balance record length and spatial fidelity, and targeted validation against SAR cases confirms that AMSR correctly captures the timing and broad footprints of polynya openings while naturally smoothing the finest frazil structure. Thus, our study bridges the gap between short, process-rich field studies and longer statistical analyses: we show that the circulation regimes invoked in process work (katabatic bursts, RAS, barrier jets) are the same regimes that dominate the multi-year EOF/MCA modes extracted from a 20-year SIC archive. This cross-scale consistency strengthens confidence that our MCA modes map to physical regimes observed in situ.

Rather than only correlating an index (e.g., ASL index) with polynya area, we show paired spatial modes that spatially cohere across fields and explain a large fraction of the SCF. This quantification supports the inference that large-scale circulation changes alter polynya behaviour primarily through the modulation of extreme coastal winds. We present this as a mechanistic linkage and we show it is consistent with both event-scale observations and decadal variability studies. By analysing RSP, TNBP and MCMP jointly, we identify that these polynyas respond differently to the same H500 anomaly — an important finding for regional process understanding and for model evaluation. For example, the same ASL displacement that intensifies southerlies and expands RSP can produce accumulation/retention in MCMP under a different regime, highlighting the need for spatially explicit model diagnostics and policy-relevant projections.

5. Conclusions

Prior long-term studies have used coarser SIC products (≈25 km) or focused on single polynyas, and process studies provide short-term mechanism tests, whereas our work is the first to combine a continuous 20-year AMSR record with MCA/EOF to diagnose how H500 anomalies map to ExWinds regimes and then to specific polynya footprints across all three RS coastal polynyas. This resolves a longstanding timescale/resolution gap in the literature.

This study used EOF analysis of 6.25×6.25 km² SIC data to identify regions of reduced concentration but high variability during peak winter, aligning with the three well-known RS polynya zones. Analysis of two decades of daily reanalysis data revealed that the leading modes of variability (~37% of SIC variance) capture both synchronous and contrasting behaviour across these zones. The dominant mode (21.5%) shows simultaneous

SIC changes in all three polynyas, while secondary modes (~7.5%) highlight north–south and east–west dipole structures linked to distinct extra-tropical circulation patterns and their influence on extreme winds over the RIS.

Modes from MCA between 500 hPa heights and extreme winds suggest that the position and intensity of geopotential height gradients, particularly those associated with shifts in the Amundsen Sea Low, modulate local wind regimes including katabatic flows, RAS, and BWCJ patterns. These wind regimes, in turn, are likely to influence SIC distribution differently across the Ross Sea, Terra Nova Bay, and McMurdo Sound polynyas. Importantly, our results show that similar RAS regimes can occur under different large-scale pressure configurations, and that the alignment of pressure gradients with the Transantarctic Mountains is a key determinant of wind direction and strength.

By resolving variability at high spatial resolution and explicitly linking large-scale circulation features to location-specific wind regimes, this work provides evidence of how synoptic-scale atmospheric patterns shape SIC variability in RS polynya zones. Our study advances understanding of how hemispheric-scale circulation and local wind dynamics jointly shape RS coastal polynyas. The results provide a baseline for model evaluation and seasonal prediction efforts, and highlight the need to capture both large-scale pressure anomalies and local wind–terrain interactions in future climate projections.

We emphasise three practical limitations. (1) Seasonal window: Our ASO focus isolates winter/spring dynamic forcing, but it excludes the full March–October polynya season — extending analyses beyond ASO (and explicitly comparing seasons) is a useful next step to capture the full thermodynamic and oceanic contributions noted by in-situ studies. (2) Ocean subsurface fields: We have not explicitly included ocean temperature/heat content or circulation in the MCA framework; given evidence that subsurface warming controls persistence (*Zhang et al., 2022*), future coupled EOF/MCA that include ocean fields (e.g., upper ocean heat content, mixed-layer depth) would help close the attribution loop. (3) SIC retrieval limits: Passive microwave SIC underestimates very low-concentration frazil bands and smooths frazil structure; therefore, while AMSR provides the requisite continuity for EOF/MCA, SAR based high-resolution products remain essential for validating process inferences. We recommend that follow-on work integrates longer in situ and ocean observations to test the multi-year persistence mechanisms. Looking ahead, this combination of multi-sensor datasets and multivariate frameworks may also lend itself well to emerging artificial intelligence and machine learning approaches, which could help capture the nonlinear, scale-dependent relationships between atmosphere, ocean, and sea ice more efficiently. We recommend that follow-on work integrates longer in-situ and ocean observations potentially within such hybrid statistical–machine learning frameworks, to better test the mechanisms underpinning multi-year persistence.

Our work suggests that both policymakers and modelers need to interpret long-term changes in RS polynya frequency/openings in the light of both atmospheric (teleconnections – SAM/ENSO) shifts and ocean subsurface changes that modulate anomaly persistence. Our results identify an atmospheric pathway and therefore provide a diagnostics framework for model evaluation and seasonal predictability studies. Coupled models should be tested for their ability to reproduce this linkage and the distinct responses of the three polynyas.

Funding:

This research is funded by the New Zealand Antarctic Science Platform (Grant Number ANTA1801) (https://www.antarcticscienceplatform.org.nz/)

Data Availability Statement

ECMWF ERA5 data were downloaded from https://cds.climate.copernicus.eu/ and the SIC data from https://seaice.uni-bremen.de/.

Acknowledgments

We thank the University of Bremen, Institute of Environmental Physics for the provision of AMSRE/2 data and European Centre for Medium-Range Weather Forecasts (ECMWF) for making fifth generation reanalysis data available for public.

References:

Ackley, S.F., Xie, H., Tichenor, E.A. et al. Sea-ice production and air/ice/ocean/biogeochemistry interactions in the Ross Sea during the PIPERS 2017 autumn field campaign. J. Phys. Oceanogr. 50, 2389–2414 (2020). https://doi.org/10.1175/JPO-D-20-0065.1

Bradtke, K.M., & Herman, A. (2023). Spatial characteristics of frazil streaks in the Terra Nova Bay Polynya from high-resolution visible satellite imagery. The Cryosphere.

Bretherton, C. S., Smith, C., & Wallace, J. M. (1992). An intercomparison of methods for finding coupled patterns in climate data. *Journal of Climate*, *5*, 541-560.

Bromwich, D. H., J. F. Carrasco, Z. Liu, and R.-Y. Tzeng (1993), Hemispheric atmospheric variations and oceanographic impacts associated with katabatic surges across the Ross ice shelf, Antarctica, J. Geophys. Res., 98(D7), 13045–13062, doi:10.1029/93JD00562.

Burada, G. K., McDonald, A., Renwick, J., & Jolly, B. (2023). Delineating Polynya Area Using Active and Passive Microwave Sensors for the Western Ross Sea Sector of Antarctica. *Remote Sensing*, *15*(10), 2545. https://doi.org/10.3390/rs15102545

Carrasco, J. F., & Bromwich, D. H. (1993). Mesoscale cyclogenesis dynamics over the southwestern Ross Sea, Antarctica. *Journal of Geophysical Research*, *98*(D7), 12973. https://doi.org/10.1029/92JD02821

Caton Harrison, T., S. Biri, T. J. Bracegirdle, J. C. King, E. C. Kent, É. Vignon, and J. Turner, 2022: Reanalysis representation of low-level winds in the Antarctic near-coastal region. Weather and Climate Dynamics, 3, 1415–1437, doi:10.5194/wcd-3-1415-2022

Carrasco, J. F., Bromwich, D. H., & Monaghan, A. J. (2003). Distribution and Characteristics of Mesoscale Cyclones in the Antarctic: Ross Sea Eastward to the Weddell Sea*. *Monthly Weather Review*, *131*(2), 289–301. https://doi.org/10.1175/1520-0493(2003)131<0289:DACOMC>2.0.CO;2

Chenoli, S. N., Turner, J., & Samah, A. A. (2012). A climatology of strong wind events at McMurdo station, Antarctica: A CLIMATOLOGY OF STRONG WIND EVENTS AT MCMURDO STATION. *International Journal of Climatology*, n/a-n/a. https://doi.org/10.1002/joc.3617

Chenoli, S. N., Turner, J., & Samah, A. A. (2015). A Strong Wind Event on the Ross Ice Shelf, Antarctica: A Case Study of Scale Interactions. *Monthly Weather Review*, *143*(10), 4163–4180. https://doi.org/10.1175/MWR-D-15-0002.1

Cohen L, Dean S, Renwick J (2013) Synoptic weather types for the Ross Sea region, Antarctica, J Clim, 26 (2): 636–649 https://doi.org/10.1175/JCLI-D-11-00690.1

Coggins, J. H. G., & McDonald, A. (2015). The influence of the Amundsen Sea Low on the winds in the Ross Sea and surroundings: Insights from a synoptic climatology. Journal of Geophysical Research: Atmospheres, 120, 2167–2189. https://doi.org/10.1002/2014JD022830

Dale, E. R., McDonald, A. J., Coggins, J. H. J., & Rack, W. (2017). Atmospheric forcing of sea ice anomalies in the Ross Sea polynya region. *The Cryosphere*, *11*(1), 267–280. https://doi.org/10.5194/tc-11-267-2017

Drucker, R., S. Martin, and R. Moritz (2003), Observations of ice thickness and frazil ice in the St. Lawrence Island polynya from satellite imagery, upward looking sonar, and salinity/temperature moorings, J. Geophys. Res., 108, 3149, doi:10.1029/2001JC001213, C5

Duffy, G. A., Montiel, F., Purich, A., & Fraser, C. I. (2024). Emerging long-term trends and interdecadal cycles in Antarctic polynyas. *Proceedings of the National Academy of Sciences*, *121*(11), e2321595121. https://doi.org/10.1073/pnas.2321595121

Eayrs, C., Li, X., Raphael, M. N., & Holland, D. M. (2021). Rapid decline in Antarctic sea ice in recent years hints at future change. *Nature Geoscience*, *14*(7), 460–464. https://doi.org/10.1038/s41561-021-00768-3

Emanuelsson, B. D., Bertler, N. A. N., Neff, P. D., Renwick, J. A., Markle, B. R., Baisden, W. T., & Keller, E. D. (2018). The role of Amundsen–Bellingshausen Sea anticyclonic circulation in forcing marine air intrusions into West Antarctica. *Climate Dynamics*, *51*(9–10), 3579–3596. https://doi.org/10.1007/s00382-018-4097-3

Fonseca, R., Francis, D., Aulicino, G., Mattingly, K. S., Fusco, G., & Budillon, G. (2023). Atmospheric controls on the Terra Nova Bay polynya occurrence in Antarctica. *Climate Dynamics*. https://doi.org/10.1007/s00382-023-06845-0

Gerrish, L., Ireland, L., Fretwell, P., & Cooper, P. (2023). High resolution vector polygons of the Antarctic coastline (7.8) [Data set]. UK Polar Data Centre, Natural Environment Research Council, UK Research & Innovation. https://doi.org/10.5285/c7fe759d-e042-479a-9ecf-274255b4f0a1

Goyal, R., Jucker, M., Sen Gupta, A., & England, M. H. (2021). Generation of the Amundsen Sea Low by Antarctic Orography. *Geophysical Research Letters*, *48*(4). https://doi.org/10.1029/2020GL091487

Guest, P.S., Persson, P.O.G., Morrison, H. et al. Inside Katabatic Winds Over the Terra Nova Bay Polynya: 1. Mobile measurements and finescale structure. J. Geophys. Res. Atmos. 126, e2021JD034902 (2021). https://doi.org/10.1029/2021JD034902

Guest, P.S., Persson, P.O.G., Morrison, H. et al. Inside Katabatic Winds Over the Terra Nova Bay Polynya: 2. Ship-based surface energy budget and fluxes. J. Geophys. Res. Atmos. 126, e2021JD034904 (2021). https://doi.org/10.1029/2021JD034904

Holland, P. R., & Kwok, R. (2012). Wind-driven trends in Antarctic sea-ice drift. *Nature Geoscience*, *5*(12), 872–875. https://doi.org/10.1038/ngeo1627

Hollands, T., & Dierking, W. (2016). Dynamics of the Terra Nova Bay Polynya: The potential of multi-sensor satellite observations. *Remote Sensing of Environment*, *187*, 30–48. https://doi.org/10.1016/j.rse.2016.10.003

Ito, M., Ohshima, K. I., Fukamachi, Y., Hirano, D., Mahoney, A. R., Jones, J., Takatsuka, T., & Eicken, H. (2019). *Favorable conditions for suspension freezing in an Arctic coastal polynya.* Journal of Geophysical Research: Oceans, 124(12), 8701–8719. https://doi.org/10.1029/2019JC015536.

Itkin, P., Spreen, G., Cheng, B., Doble, M., Girard-Ardhuin, F., Haapala, J., et al. (2017). Thin ice and storms: Sea ice deformation from buoy arrays deployed during N-ICE2015. *Journal of Geophysical Research: Oceans*, *122*(6), 4661–4674. https://doi.org/10.1002/2016JC012403

Jacobs, S.S. and C.F. Giulivi (1998). Interannual Ocean and Sea Ice Variability in the Ross Sea. In Ocean, Ice, and Atmosphere: Interactions at the Antarctic Continental Margin (eds. S.S. Jacobs and R.F. Weiss), American Geophysical Union, Washington, D.C., doi: 10.1029/AR075p0135.

Jena, B., Bajish, C. C., Turner, J., Ravichandran, M., Anilkumar, N., & Kshitija, S. (2022). Record low sea ice extent in the Weddell Sea,Antarctica in April/May 2019 driven by intense and explosive polar cyclones. Npj Climate and Atmospheric Science, 5(1), 19. https://doi.org/10.1038/s41612-022-00243-9

Jolliffe, I. T. (2003). A Cautionary Note on Artificial Examples of EOFs. Retrieved from https://journals.ametsoc.org/view/journals/clim/16/7/1520-0442_2003_016_1084_acnoae_2.0.co_2.xml

Josey, S. A., Meijers, A. J. S., Blaker, A. T., Grist, J. P., Mecking, J., Ayres, H. C., … (2024). *Record-low Antarctic sea ice in 2023 increased ocean heat loss and storms.* Nature, 636, 635–639. https://doi.org/10.1038/s41586-024-08368-y

Kwok, R. (2005). Ross Sea Ice Motion, Area Flux, and Deformation. *Journal of Climate*, *18*(18), 3759–3776. https://doi.org/10.1175/JCLI3507.1

Lachlan-Cope, T., & Connolley, W. (2016). Teleconnections between the tropical Pacific and the Amundsen-Bellinghausens Sea: Role of the El Niño/Southern Oscillation. https://doi.org/10.1029/2005JD006386

Laxon, S. W., Ridout, A. L., Barber, D. G., & Van den Broeke, M. R. (2013). CryoSat-2 estimates of Antarctic sea ice thickness. *Geophysical Research Letters*, 40(11), 2578–2583. https://doi.org/10.1002/grl.5056Lian, T., & Chen, D. (2012). An Evaluation of Rotated EOF Analysis and Its Application to Tropical Pacific SST Variability. *Journal of Climate*, *25*(15), 5361–5373. https://doi.org/10.1175/JCLI-D-11-00663.1

Martin, S., Drucker, R., & Kwok, R. Sea-ice production and export from coastal polynyas in the Weddell and Ross Seas. Geophys. Res. Lett. 31, L15306 (2004). https://doi.org/10.1029/2003GL017953

McDonald, A. J., & Cairns, L. H. (2020). A New Method to Evaluate Reanalyses Using Synoptic Patterns: An Example Application in the Ross Sea/Ross Ice Shelf Region. *Earth and Space Science*, *7*(1), e2019EA000794. https://doi.org/10.1029/2019EA000794

Melsheimer, Christian, & Spreen, Gunnar. (2020). AMSR-E ASI sea ice concentration data, Antarctic, version 5.4 (NetCDF) (June 2002 - September 2011) [Text/tab-separated-values]. PANGAEA - Data Publisher for Earth & Environmental Science. https://doi.org/10.1594/PANGAEA.919778

Meng, Z. (2023, July 25). SACPY -- A Python Package for Statistical Analysis of Climate (Version 0.0.19). Zenodo. https://doi.org/10.5281/zenodo.8182411

Mezgec, K., Stenni, B., Crosta, X., Masson-Delmotte, V., Baroni, C., Braida, M., et al. (2017). Holocene sea ice variability driven by wind and polynya efficiency in the Ross Sea. *Nature Communications*, *8*(1), 1334. https://doi.org/10.1038/s41467-017-01455-x

Mo, R. P. (2003). Efficient algorithms for maximum covariance analysis of datasets with many variables and fewer realizations: A revisit. *Journal of Atmospheric and Oceanic Technology*, 20(12), 1804-1809.

Morales Maqueda, M. A., A. J. Willmott, and N. R. T. Biggs (2004), Polynya dynamics: A review of observations and modeling, Rev. Geophys., 42, RG1004, doi:10.1029/2002RG000116.

Murphy, B. F., and I. Simmonds, 1993: An Analysis of Strong Wind Events Simulated in a GCM near Casey in the Antarctic. *Mon. Wea. Rev.*, **121**, 522–534, https://doi.org/10.1175/1520-0493(1993)121<0522:AAOSWE>2.0.CO;2.

Murphy, B. F., 2003: Prediction of Severe Synoptic Events in Coastal East Antarctica. *Mon. Wea. Rev.*, **131**, 354–370, https://doi.org/10.1175/1520-0493(2003)131<0354:POSSEI>2.0.CO;2.Nakata, K., Ohshima, K. I., & Nihashi, S. (2021). Mapping of active frazil for Antarctic coastal polynyas, with an estimation of sea-ice production. Geophysical Research Letters, 48, e2020GL091353. https://doi.org/10.1029/2020GL091353

Nigro, M. A., & Cassano, J. J. (2014). Identification of Surface Wind Patterns over the Ross Ice Shelf, Antarctica, Using Self-Organizing Maps. *Monthly Weather Review*, *142*(7), 2361–2378. https://doi.org/10.1175/MWR-D-13-00382.1

Nicolas, J. P., and D. H. Bromwich, 2011: Climate of West Antarctica and Influence of Marine Air Intrusions. J. Climate, 24, 49–67, https://doi.org/10.1175/2010JCLI3522.1

North, G. R., Bell, T. L., Cahalan, R. F., & Moeng, F. J. (1982). Sampling Errors in the Estimation of Empirical Orthogonal Functions. *Monthly Weather Review*, *110*(7), 699–706. https://doi.org/10.1175/1520-0493(1982)110<0699:SEITEO>2.0.CO;2

O'Connor, W. P., Bromwich, D. H., & Carrasco, J. F. (1994). Cyclonically Forced Barrier Winds along the Transantarctic Mountains near Ross Island. *Monthly Weather Review*, *122*(1), 137–150. https://doi.org/10.1175/1520-0493(1994)122<0137:CFBWAT>2.0.CO;2

Organization (WMO), W. M. (n.d.). WMO Sea-Ice Nomenclature. Retrieved February 19, 2024, from https://library.wmo.int/records/item/41953-wmo-sea-ice-nomenclature

Parish, T. R., & Bromwich, D. H. (1998). A Case Study of Antarctic Katabatic Wind Interaction with Large-Scale Forcing. *Monthly Weather Review*, *126*(1), 199–209. https://doi.org/10.1175/1520-0493(1998)126<0199:ACSOAK>2.0.CO;2

Parish, T. R., J. J. Cassano, and M. W. Seefeldt (2006), Characteristics of the Ross Ice Shelf air stream as depicted in Antarctic Mesoscale Prediction System simulations, J. Geophys. Res., 111, D12109, doi:10.1029/2005JD006185.

Park, J., Kim, H.-C., Jo, Y.-H., Kidwell, A., & Hwang, J. (2018). Multi-temporal variation of the Ross Sea Polynya in response to climate forcings. *Polar Research*, *37*(1), 1444891. https://doi.org/10.1080/17518369.2018.1444891

Paul, S., Lengaigne, M., & Vialard, J. (2013). Impact of wind variability on sea ice export in the Southern Ocean. *Geophysical Research Letters*, 40(6), 1063–1067. https://doi.org/10.1002/grl.50216

Rack, W., Price, D., Haas, C., Langhorne, P. J., & Leonard, G. H. (2021). Sea Ice Thickness in the Western Ross Sea. *Geophysical Research Letters*, *48*(1), e2020GL090866. https://doi.org/10.1029/2020GL090866

Raphael, M. N., and Coauthors, 2016: The Amundsen Sea Low: Variability, Change, and Impact on Antarctic Climate. *Bull. Amer. Meteor. Soc.*, **97**, 111–121, https://doi.org/10.1175/BAMS-D-14-00018.1.

Raphael, M. N., Holland, M. M., Landrum, L., & Hobbs, W. R. (2019). Links between the Amundsen Sea Low and sea ice in the Ross Sea: seasonal and interannual relationships. *Climate Dynamics*, *52*(3–4), 2333–2349. https://doi.org/10.1007/s00382-018-4258-4

Renwick, J. A. (2005). Persistent Positive Anomalies in the Southern Hemisphere Circulation. *Monthly Weather Review*, *133*(4), 977–988. https://doi.org/10.1175/MWR2900.1

Renwick, J. A., & Revell, M. J. (1999). Blocking over the South Pacific and Rossby Wave Propagation. *Monthly Weather Review*, *127*(10), 2233–2247. https://doi.org/10.1175/1520-0493(1999)127<2233:BOTSPA>2.0.CO;2

Rieger, N., Corral, Á., Olmedo, E., & Turiel, A. (2021). Lagged teleconnections of climate variables identified via complex rotated Maximum Covariance Analysis. *Journal of Climate*, 1–59. https://doi.org/10.1175/JCLI-D-21-0244.1

Schroeter, S., O'Kane, T. J., & Sandery, P. A. (2023). Antarctic sea ice regime shift associated with decreasing zonal symmetry in the Southern Annular Mode. *The Cryosphere*, *17*(2), 701–717. https://doi.org/10.5194/tc-17-701-2023

Schwerdtfeger, W. (1975), The effect of the Antarctic Peninsula on the temperature regime of the Weddell Sea, *Mon. Weather Rev.*, **103**, 41–51.

Seefeldt, M. W., Cassano, J. J., & Parish, T. R. (2007). Dominant Regimes of the Ross Ice Shelf Surface Wind Field during Austral Autumn 2005. *Journal of Applied Meteorology and Climatology*, *46*(11), 1933–1955. https://doi.org/10.1175/2007JAMC1442.1

Seefeldt, M. W., and J. J. Cassano (2012), A description of the Ross Ice Shelf air stream (RAS) through the use of self-organizing maps (SOMs), J. Geophys. Res., 117, D09112, doi:10.1029/2011JD016857.

Stammerjohn, S. E., Maksym, T., & Martinson, D. G. (2008). Sea ice in the Southern Ocean: The Weddell Sea and Ross Sea. Progress in Oceanography, 78(3-4), 375–394. https://doi.org/10.1016/j.pocean.2008.02.002

Tamura, T., Ohshima, K.I., & Nihashi, S. Mapping of sea ice production for Antarctic coastal polynyas. Geophys. Res. Lett. 35, L07606 (2008). https://doi.org/10.1029/2007GL032903

Thomas, E. R., & Abram, N. J. (n.d.). Ice core reconstruction of sea ice change in the Amundsen-Ross Seas since 1702 A.D. https://doi.org/10.1002/2016GL068130

Thompson, L., Smith, M., Thomson, J., Stammerjohn, S., Ackley, S., & Loose, B. (2020). Frazil ice growth and production during katabatic wind events in the Ross Sea, Antarctica. *The Cryosphere*, *14*(10), 3329–3347. https://doi.org/10.5194/tc-14-3329-2020

Turner, J., Bromwich, D., Colwell, S., Dixon, S., Gibson, T., Hart, T., et al. (1996). The Antarctic First Regional Observing Study of the Troposphere (FROST) Project. *Bulletin of the American Meteorological Society*, *77*(9), 2007–2032. https://doi.org/10.1175/1520-0477(1996)077<2007:TAFROS>2.0.CO;2

Turner, J., Phillips, T., Hosking, J. S., Marshall, G. J., & Orr, A. (2013). The Amundsen Sea low: The Amundsen Sea low. *International Journal of Climatology*, *33*(7), 1818–1829. https://doi.org/10.1002/joc.3558

Voropayev, S. I., H. J. S. Fernando, and L. A. Mitchell, 1995: On the Rate of Frazil Ice Formation in Polar Regions in the Presence of Turbulence. *J. Phys. Oceanogr.*, **25**, 1441–1450, https://doi.org/10.1175/1520-0485(1995)025<1441:OTROFI>2.0.CO;2.

Wallace, J. M., Smith, C., & Bretherton, C. S. (1992). Singular Value Decomposition of Wintertime Sea Surface Temperature and 500-mb Height Anomalies. *Journal of Climate*, *5*(6), 561–576. https://doi.org/10.1175/1520-0442(1992)005<0561:SVDOWS>2.0.CO;2

Weber, N. J., Lazzara, M. A., Keller, L. M., and Cassano, J. J.: The extreme wind events in the ross island region of Antarctica, Weather Forecast., 31, 985–1000, 2016. a

Wenta, M., & Cassano, J.J. (2020). The Atmospheric Boundary Layer and Surface Conditions during Katabatic Wind Events over the Terra Nova Bay Polynya. Remote. Sens., 12, 4160.

Wilks, D. S. (2011). *Statistical Methods in the Atmospheric Sc^{ie}nces* (3rd ed., Vol. 100). Academic Press.sss

Williams, G. D., N. L. Bindoff, S. J. Marsland, and S. R. Rintoul (2008), Formation and export of dense shelf water from the Adélie Depression, East Antarctica, J. Geophys. Res., 113, C04039, doi:10.1029/2007JC004346.

Yuan, N., Ding, M., Ludescher, J., & Bunde, A. (2017). Increase of the Antarctic Sea Ice Extent is highly significant only in the Ross Sea. *Scientific Reports*, *7*, 41096. https://doi.org/10.1038/srep41096

Zhang, L., Delworth, T. L., Yang, X., Zeng, F., Lu, F., Morioka, Y., & Bushuk, M. (2022). The relative role of the subsurface Southern Ocean in driving negative Antarctic Sea ice extent anomalies in 2016–2021. *Communications Earth & Environment*, *3*(1), 1–9. https://doi.org/10.1038/s43247-022-00624-1

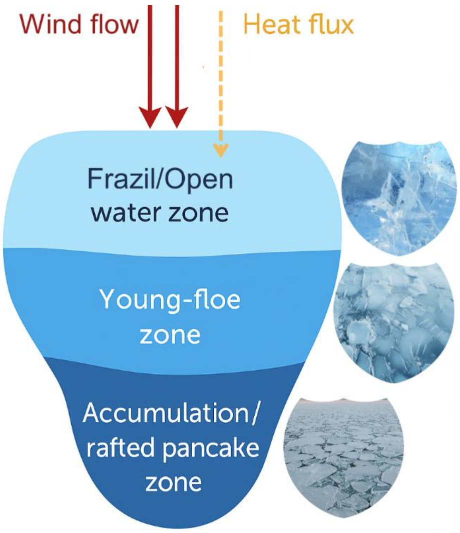

Conceptual Model of Wind and Heat Flux Controls on Polynya Sea-Ice Formation

https://doi.org/10.5194/egusphere-2025-5369
Preprint. Discussion started: 21 January 2026

Ppaer figures

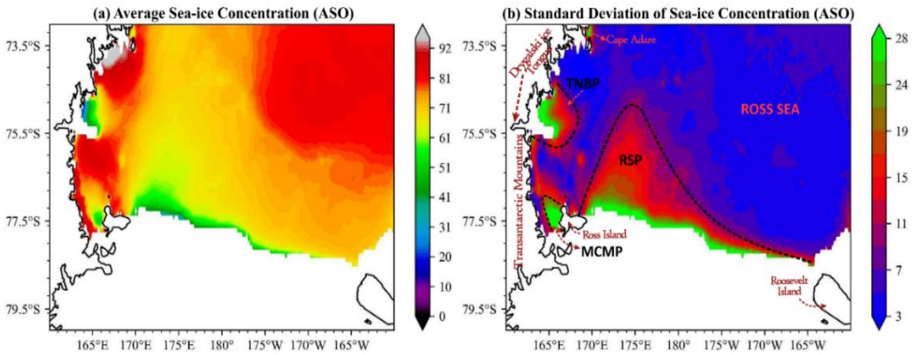

Figure 1: (a)Average SIC (percentage, on left) and (b) Standard Deviation of SIC during ASO for the period 2002-2022 (polynya regions are enclosed in black-dotted lines in 1b)

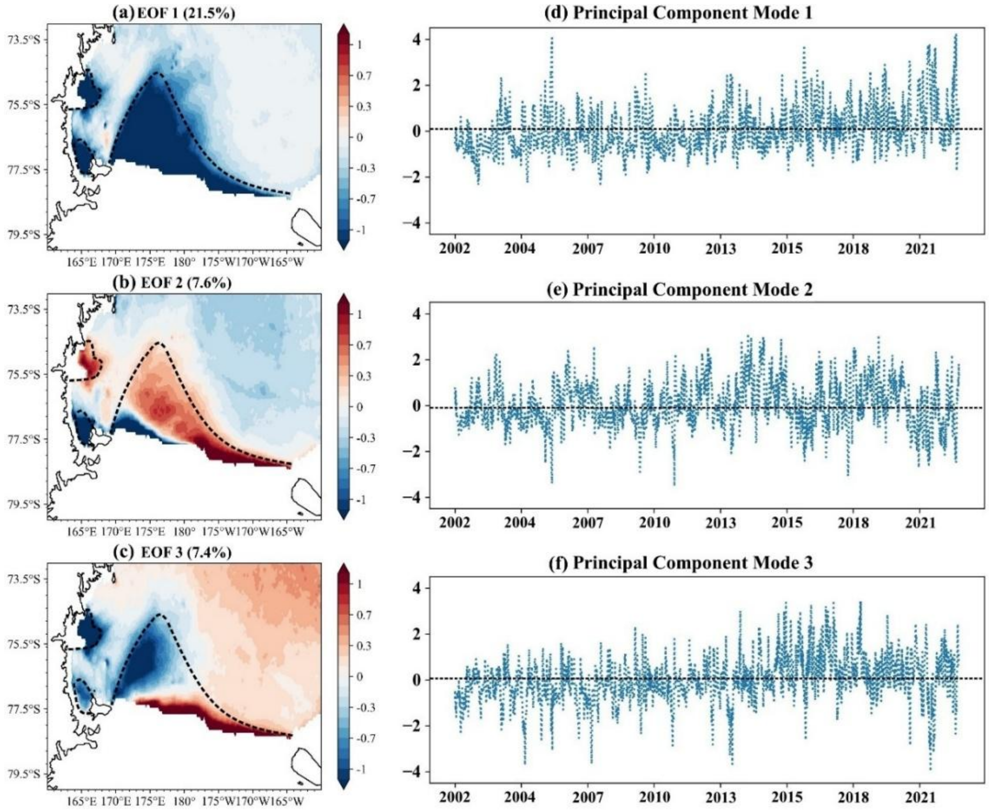

Figure 2: First three EOF modes derived from AMSRE/2 SIC data for the ASO (Spatial patterns on left (a-c) and PCs on right (d-f)). Black dotted lines represent standard deviation threshold from Figure 1(b).

639

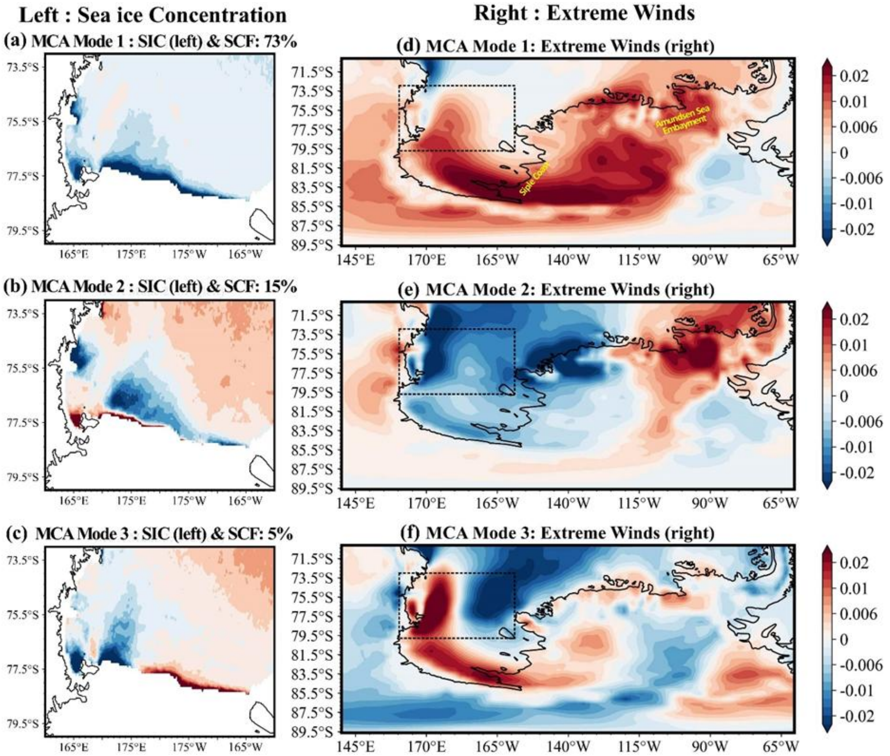

640
641 Figure 3A: Leading MCA spatial patterns (Top to bottom) of SIC/ExWinds (left: SIC and right: Extreme Winds).
642 Covarying patterns spatially in Mode 1 are shown in panels (a) and (d), mode 2 in (b) and (e), and mode 3 in (c)
643 and (f)

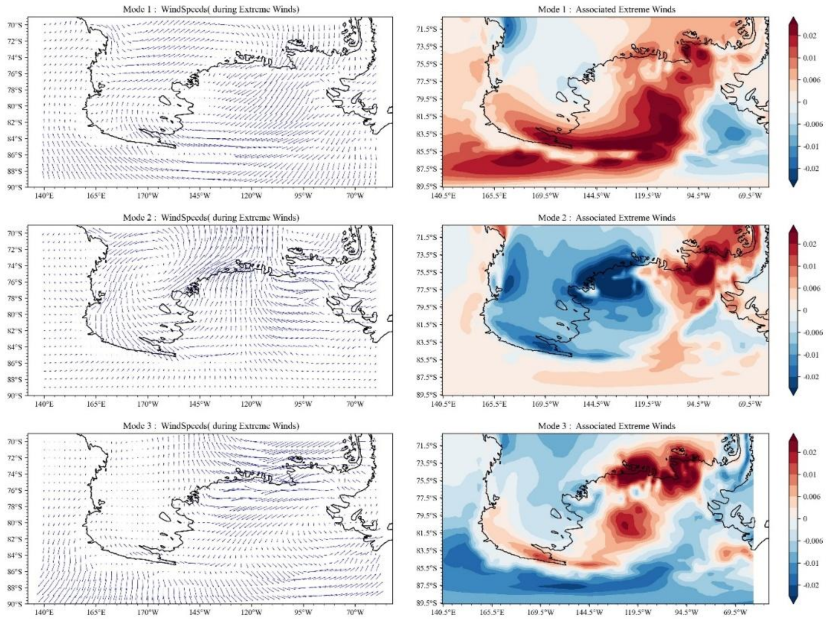

Figure 3B: Extreme Winds and Large-scale wind vectors to demonstrate wind directions

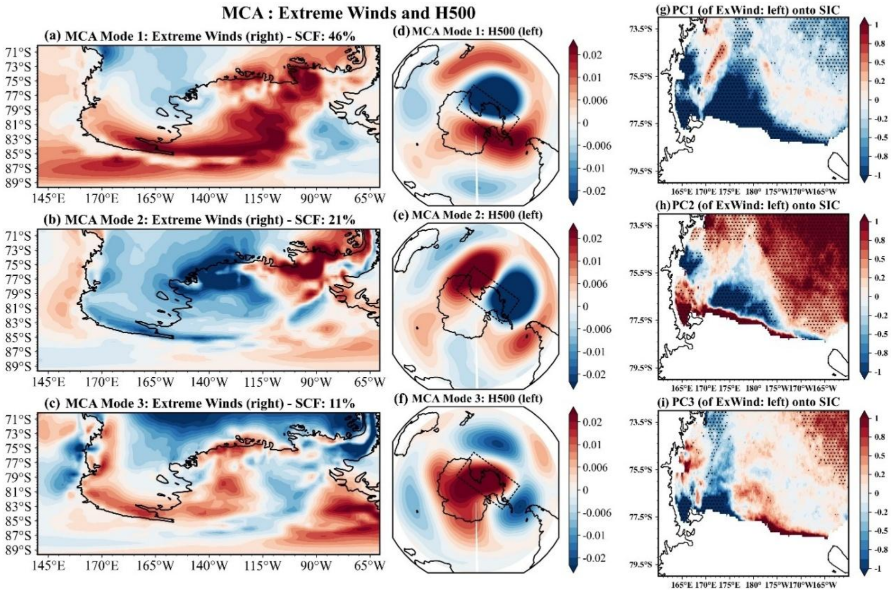

Figure 4: Leading MCA modes of Extreme Winds (1st column) and H500 (2nd column). 3rd column represents regressions (p-value 0.005) from PCs of ExWin (MCA: ExWin/H500) on SIC anomalies